NASA TECHNICAL NOTE

NASA TN D-3691

C.1

NASA TN D-3691

EXPERIMENTAL INVESTIGATION OF THE PRESSURE CHARACTERISTICS OF NONWETTING, CONDENSING FLOW OF MERCURY IN A SODIUM-POTASSIUM-COOLED, TAPERED TUBE

by Richard W. Vernon, Roy A. Lottig, and William D. Kenney

Lewis Research Center
Cleveland, Ohio

NATIONAL AERONAUTICS AND SPACE ADMINISTRATION • WASHINGTON, D. C. • NOVEMBER 1966

NASA TN D-3691

EXPERIMENTAL INVESTIGATION OF THE PRESSURE CHARACTERISTICS OF NONWETTING, CONDENSING FLOW OF MERCURY IN A SODIUM-POTASSIUM-COOLED, TAPERED TUBE

By Richard W. Vernon, Roy A. Lottig, and William D. Kenney

Lewis Research Center
Cleveland, Ohio

NATIONAL AERONAUTICS AND SPACE ADMINISTRATION

For sale by the Clearinghouse for Federal Scientific and Technical Information
Springfield, Virginia 22151 – Price $2.00

EXPERIMENTAL INVESTIGATION OF THE PRESSURE CHARACTERISTICS OF NONWETTING, CONDENSING FLOW OF MERCURY IN A SODIUM-POTASSIUM-COOLED, TAPERED TUBE

by Richard W. Vernon, Roy A. Lottig, and William D. Kenney

Lewis Research Center

SUMMARY

Local mercury static pressures were measured for the nonwetting two-phase flow of mercury condensing in a NaK-cooled, counterflow, tapered tube heat exchanger. The relations of the mercury inlet static pressure and overall static-pressure change were obtained experimentally as functions of condensing length. The inside diameter of the tapered tube (0.035-in.-thick wall) decreased from 0.460 inch at the mercury inlet to 0.20 inch at a location 40 inches downstream from the inlet. The mercury and NaK flow rates were nominally 155 and 515 pounds per hour, respectively. The range of tube inlet mercury vapor velocities was 110 to 155 feet per second. The correlation of Lockhart and Martinelli used with assumed liquid-to-vapor velocity ratios of 0, 0.5, and 1.0, and the Koestel, et al. fog flow correlation, used with a liquid-to-vapor velocity ratio of 1.0, were employed to calculate static-pressure profiles, which were compared with the measured static pressures.

The mercury inlet static pressure varied from 16 to 22 pounds per square inch absolute and exhibited high sensitivity to changes of condensing length between 7 and 16 inches and relative low sensitivity to changes in condensing lengths between 16 and 34 inches.

The Lockhart-Martinelli correlation, with assumed liquid-to-vapor velocity ratios of 0.5 and 1.0, and the fog flow model of Koestel, et al. predicted axial static-pressure profiles that generally agreed with the measured static pressures in the first 75 percent of the condensing length. For the last 25 percent of the condensing length, the two-phase friction coefficients Φ_g predicted by both correlations appeared low.

The experimental overall mercury static-pressure difference (from inlet to outlet) varied from a small pressure rise (about 0.5 psi) for condensing lengths less than 20 inches to a small pressure drop (about 0.5 psi), which occurred at a condensing length of 34 inches. The predicted pressures, which used the pressure drop correlations of Lockhart and Martinelli and Koestel, et al. resulted in overall static-pressure changes which indicated more pressure rise than was found experimentally.

INTRODUCTION

One of the more promising concepts for generating electrical energy in the kilowatt and megawatt power range for long term space flight missions is the Rankine cycle nuclear powerplant typified by the SNAP-8 system. A characteristic of Rankine systems is the phase changes of the working fluid during the heating and heat rejection portions of the cycle. In the SNAP-8 system, which utilizes mercury as the working fluid, the mercury vapor is exhausted from the turbine into the condenser where thermal energy is removed from the mercury by a eutectic mixture of sodium and potassium (NaK) and is subsequently rejected from the system to space by means of a liquid radiator. The SNAP-8 condenser is a counter flow heat exchanger with the mercury vapor being condensed inside 73 tapered diameter tubes.

Accurate predictions of the condenser inlet and outlet pressures are necessary to assure compatibility of the condenser component with the design requirements of its neighboring turbine and pump components. Because the condenser inlet pressure and turbine outlet pressure are directly related, the turbine performance can be adversely affected if the condenser inlet pressure becomes greater than the design turbine outlet pressure. Equally important considerations are the serious cavitation damage and instability that can occur in the liquid pump if the condenser outlet pressure is not sufficiently high to provide the required net positive suction pressure at the pump inlet.

Thus, one of the critical problems encountered in the design of the condenser component is the definition of the pressure characteristics of the two-phase flow in the condenser. In particular, the pressure level of the working fluid in the condenser is related to the heat transfer characteristics of the working fluid and condenser coolant and the liquid inventory in the condenser. The heat transfer characteristics of the liquid metals proposed as working fluids and coolants are not accurately defined. In addition, two-phase frictional pressure gradients and momentum gradients are needed to determine the outlet pressure once the condenser inlet pressure is known. Several analytical methods have been developed for predicting the frictional pressure gradients for the two-phase flow of working fluids (refs. 1 to 3). However, because of the difficulties of accurately defining analytical flow models that fully describe a condensing process of continuously varying quality, significant disagreements exist between predicted and measured axial static-pressure distributions in a condenser tube (ref. 4). In recognition of these problems, an experimental investigation was conducted at the Lewis Research Center; the test section and conditions for this investigation were chosen to approximate the design conditions that would be encountered by a single typical tube in the SNAP-8 condenser.

The main objective of this report is to present experimental data that were obtained to define the inlet pressure and pressure drop characteristics for nonwetting mercury flow in a single, tapered diameter tube cooled by NaK. In addition, the experimental data were compared to the predicted static-pressure profiles obtained by employing the correlations proposed by Lockhart-Martinelli and Koestal, et al.

APPARATUS

The mercury and NaK loops are shown schematically in figure 1. Liquid mercury was stored in the expulsion unit where it was pressurized with argon gas. The liquid mercury flow rate was determined by measuring the pressure drop across a calibrated orifice located at the outlet of the expulsion unit. Boiling of the mercury occurred in three stages. The liquid was first heated to the approximate saturation temperature in the preheater. This unit consisted of 4 feet of coiled stainless-steel tubing which was heated electrically. The liquid mercury then entered the high heat flux unit where conditions were imposed to initiate nucleate boiling, resulting in a quality of approximately 25 percent. This unit consisted of 10 feet of stainless-steel tubing fitted into an electrically heated aluminum block. The mixture then entered the main boiler. The boiler unit consisted of a helical flattened tube that formed the mercury flow passage. Electrical power was applied directly to the flattened tube which served as a resistance heater. The mixture was then passed from the tubing into a plenum chamber, which was partially filled with stainless-steel cuttings to minimize liquid carryover. The vapor superheat was removed in a NaK-cooled desuperheater where the NaK temperature was maintained approximately 5° F above the mercury saturation temperature to avoid condensing the mercury vapor. The mercury vapor then passed through a venturi flowmeter prior to entering the condensing test section.

The condensing test section was a counterflow, tube-in-shell, heat exchanger. The tube, through which the condensing mercury flowed, was made of 9 chromium (Cr), 1 molybdenum (Mo) alloy stainless steel with a 0.035-inch-thick wall. This tube was uniformly tapered from 0.46 to 0.20 inch (nominal inside diameters) over a length of 40 inches. Approximately 12 inches of length having a constant 0.20-inch inside diameter was welded to the small end of the tube. The outer tube, which formed the annulus through which the NaK coolant flowed, was also tapered and was made of 316 stainless steel with a 0.035-inch-thick wall. The taper of the outer tube was the same as that of

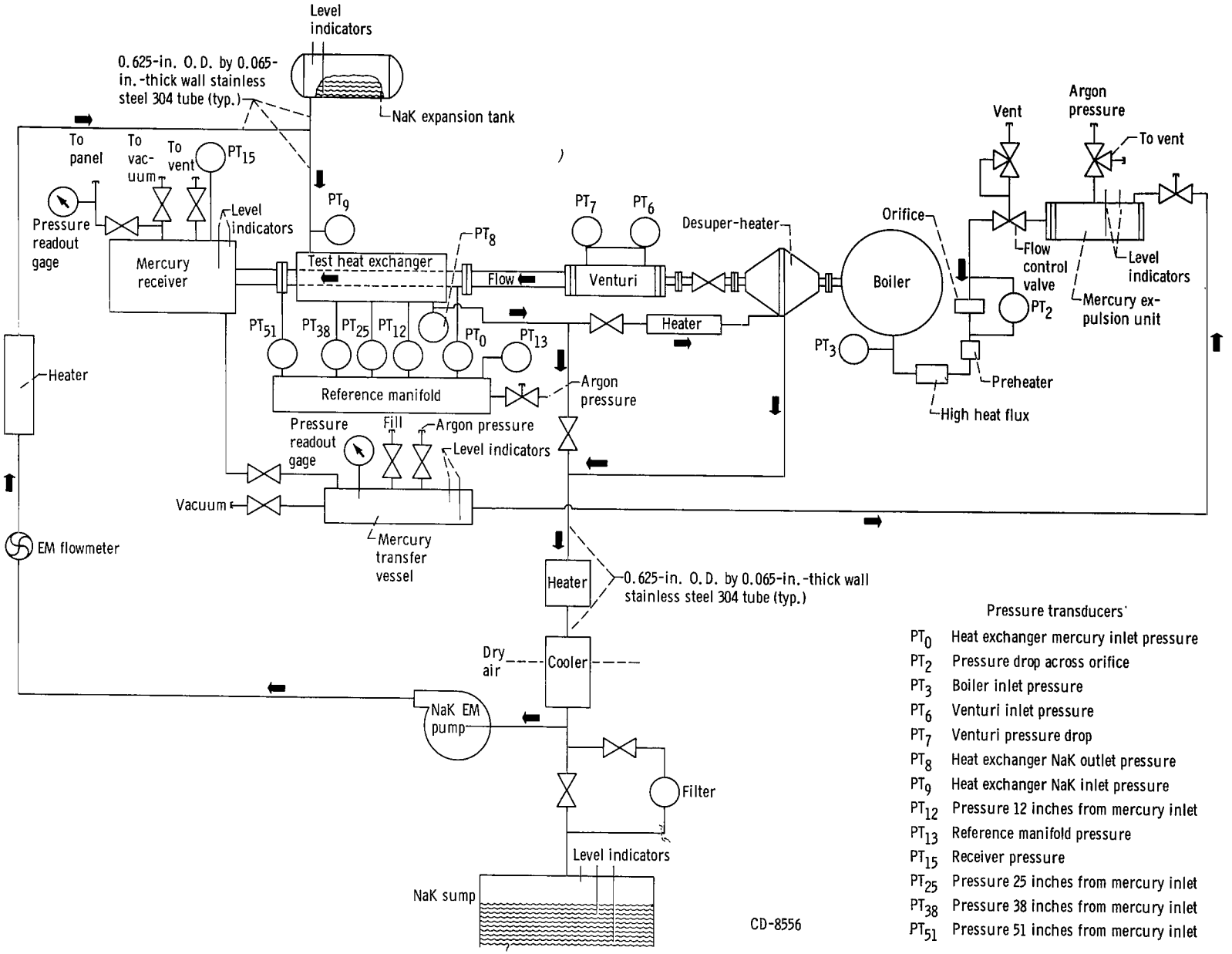

Pressure transducers

PT_0	Heat exchanger mercury inlet pressure
PT_2	Pressure drop across orifice
PT_3	Boiler inlet pressure
PT_6	Venturi inlet pressure
PT_7	Venturi pressure drop
PT_8	Heat exchanger NaK outlet pressure
PT_9	Heat exchanger NaK inlet pressure
PT_{12}	Pressure 12 inches from mercury inlet
PT_{13}	Reference manifold pressure
PT_{15}	Receiver pressure
PT_{25}	Pressure 25 inches from mercury inlet
PT_{38}	Pressure 38 inches from mercury inlet
PT_{51}	Pressure 51 inches from mercury inlet

Figure 1. - System with mercury and NaK loops.

the inner tube, maintaining a 0.103-inch annulus between the two tubes.

Liquid mercury from the condenser outlet flowed into a receiver which in turn drained into a transfer vessel. The transfer vessel, when isolated from the receiver by a valve, was pressurized to transfer mercury back into the expulsion unit.

The main NaK loop can be traced in figure 1, starting at the electromagnetic pump. The NaK flow rate was measured by an electromagnetic flowmeter. The NaK then flowed through the test section counter to the mercury flow and then into the desuperheater. An electrical heater between the test section and desuperheater was used to maintain the NaK temperature into the desuperheater approximately 5° F above the mercury saturation temperature. From the desuperheater the NaK returned to the pump. An air cooler removing heat from the NaK, provided a coarse temperature control. Fine temperature control was obtained by electrical heaters.

INSTRUMENTATION

The location and calibration range of the pressure transducers used in this investigation can be found in table I. The location of the temperature and pressure instrumentation on the test section is shown in figure 2. The skin thermocouples on the outer shell were spot welded to the 316 stainless-steel tube at 1-inch intervals. These thermocouples were used to measure local wall temperatures and indicate the mercury interface

TABLE I. - TRANSDUCER CALIBRATION RANGES

Pressure transducer	Description	Calibration range, psi
PT_2	Pressure drop across orifice	[a]0 to 80
PT_3	Boiler inlet pressure	[b]0 to 200
PT_6	Venturi inlet pressure	[b]0 to 32
PT_7	Venturi pressure drop	[a]0 to 5
PT_8	Heat exchanger NaK outlet pressure	[b]0 to 50
PT_9	Heat exchanger NaK inlet pressure	[b]0 to 50
PT_{13}	Reference manifold pressure	[a]0 to 24
PT_{15}	Receiver pressure	[b]0 to 32
PT_0	Heat exchanger mercury inlet pressure	[a]0 to 10
PT_{12}	Pressure 12 inches from mercury inlet	[a]0 to ±5
PT_{25}	Pressure 25 inches from mercury inlet	[a]0 to ±5
PT_{38}	Pressure 38 inches from mercury inlet	[a]0 to ±5
PT_{51}	Pressure 51 inches from mercury inlet	[a]0 to 10

[a]Differential.
[b]Absolute.

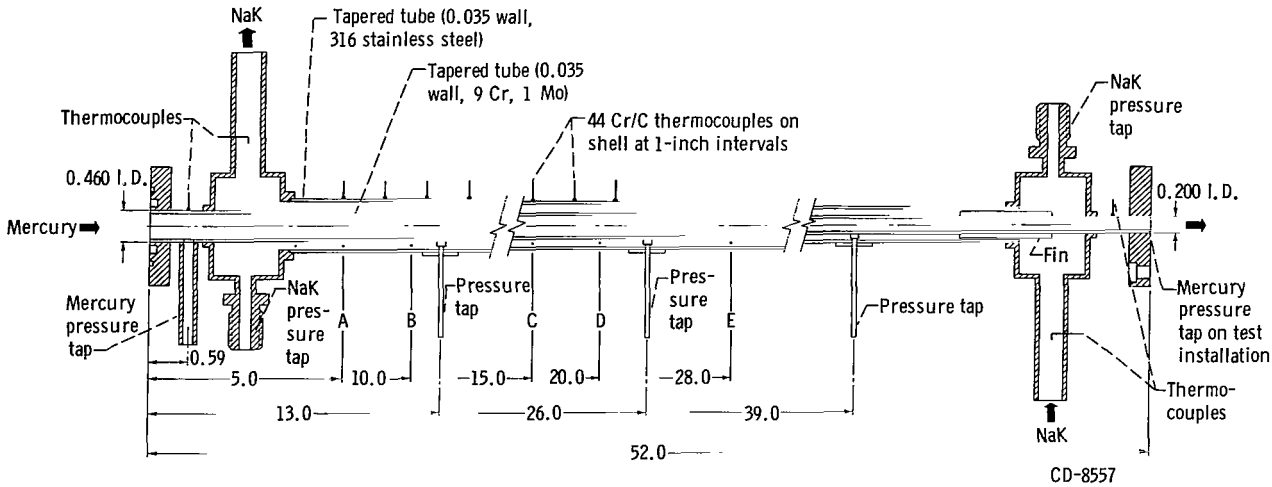

Figure 2. - Test section instrumentation. (A, B, C, D, and E are NaK stream thermocouple sections. All dimensions in inches.)

position.

Immersed sheathed thermocouples were used in the measurement of the NaK stream temperatures. These thermocouples were placed in the middle of the 0.103-inch annulus at three circumferential points, 90° apart, at each station, with a total of five stations. In addition to being sheathed, the thermocouple used for measuring the mercury vapor temperature in the venturi was provided with a thin stainless-steel strip which acted as a shield to prevent liquid droplets from impinging upon the sensing element. All temperatures were measured by chromel-constantan thermocouples.

Mercury static-pressure taps were located 0.4 inch upstream of the condenser inlet and 12, 25, 38, and 51 inches from the condenser inlet. The transducers at the 0.4- and 51-inch stations were used as the condenser inlet and outlet pressures, respectively, and had a differential pressure range of ±10 pounds per square inch, while those at the 12-, 25-, and 38-inch stations had a differential pressure range of ±5 pounds per square inch. They were all connected to the test section by a short horizontal tube to minimize liquid head effects. The reference side of the pressure transducers were all connected to a regulated pressure manifold, providing a measured reference pressure.

PROCEDURE

A calibration procedure similar to that described in reference 5 was used. Prior to each data run, a complete calibration of the absolute and differential pressure transducers was carried out. The transducers were calibrated with the short horizontal coupling tube and transducer cavity filled with liquid mercury. All condenser differential pressure transducers were calibrated simultaneously by pressurizing the mercury system with

gaseous nitrogen through the venturi. The low pressure sides were all opened to atmospheric pressure, and a selected range of pressures was applied to the system. The desired oscillograph and readout gage spans were adjusted, and recorded runs were made over the calibration range so that transducer calibration curves could be plotted. The absolute pressure transducers were also calibrated simultaneously by applying pressure to the entire system. The zero reference for these transducers was obtained with the system pumped down to a vacuum of approximately 1 torr.

With the NaK lines filled, power was applied to the electromagnetic pump to start circulation. The NaK flow rate was indicated by a digital readout from the electromagnetic flowmeter. The NaK was heated to approximately 650° F by two heaters. The mercury loop, meanwhile, was being evacuated to approximately 0.2 torr and the mercury heaters were brought to operating temperatures.

With all temperatures at the desired level, the mercury preheater was turned on and mercury flow started. Flow rate was controlled by an automatic flow control valve that was operated by the signal from the transducer measuring the pressure drop across the calibrated orifice.

Initially the mercury flow rate was set at 0.03 pound per second, and mercury vapor was allowed to purge the system for approximately 3 minutes to remove remaining noncondensables from the lines. The NaK flow rate and inlet temperature were set, and the mercury receiver pressure was adjusted to locate the interface at the desired position. During loop operation, the interface location was indicated by the NaK shell temperature profile, which was displayed on a profile monitor.

On another NaK-cooled test section with a thinner wall, the location of the liquid vapor interface, as determined by the temperature profile, was checked by using an X-ray unit. The two methods of determining the interface location agreed to within ±1 inch.

METHOD OF ANALYSIS

Static pressures were calculated, employing the two-phase friction correlations of Lockhart-Martinelli and Koestel, et al. (ref. 1 and 2), and were compared to the measured static pressures. The predicted mercury static pressures were calculated by iteration in 1-inch increments from the condenser tube inlet to the mercury liquid-vapor interface. The static-pressure change for an increment of two-phase flow, if the effects of liquid droplet drag are neglected, is

$$\Delta P_s = \Delta P_{TPF} + \Delta P_{mom} \tag{B1}$$

(A list of symbols is given in appendix A.) To calculate the static-pressure changes, saturation conditions were assumed and the physical properties of the liquid and vapor, obtained from reference 6, were assumed constant for the increment being considered. For the first increment the physical properties were obtained as a function of the measured inlet static pressure. The two-phase frictional pressure change and the pressure change due to momentum change were then calculated for the first increment. The net pressure change was then subtracted from the inlet pressure to obtain the pressure at the beginning of the next increment. The iterative calculations were continued until the static pressure at the liquid-vapor interface was determined.

Two correlations were chosen to calculate the two-phase frictional pressure changes. One of the correlations chosen, proposed by Lockhart and Martinelli, is based upon data obtained for isothermal two-phase, two-component flow. The other correlation, proposed by Koestal, et al. is based upon a theoretical fog flow model.

The two-phase frictional pressure changes for both correlations were obtained from the following general expression:

$$\Delta P_{TPF} = \Phi_g^2 \left(\frac{dP_g}{dL} \right) \Delta L \tag{B3}$$

where

$$\Phi_g^2 \equiv \frac{\left(\frac{dP_{TPF}}{dL} \right)}{\left(\frac{dP_g}{dL} \right)}$$

There is, however, a basic difference between the two correlations in the evaluation of Φ_g. In the Lockhart-Martinelli correlation (ref. 1) the parameter Φ_g is determined empirically as a function of χ; the parameter χ is a function of the quality and the physical properties and flow regimes of both the liquid and vapor. In the theoretical fog flow model (ref. 2) the parameter Φ_g is shown to be a function of the vapor quality and the Weber number of the mercury. The methods used to determine the values of Φ_g for both correlations are presented in appendix B.

The pressure change due to momentum change was also required to evaluate the predicted static-pressure change. Both the liquid and vapor velocities were needed to determine the predicted momentum changes. It was possible to calculate the vapor phase velocity but not the liquid phase velocity. Therefore, for the Lockhart-Martinelli correlation, three liquid-to-vapor velocity ratios were assumed to determine the effect of the various liquid velocities on the theoretical pressure change. The three velocity ratios chosen are 1.0, 0.5, and 0.0. Koestel, et al. recommend an assumed velocity ratio of

1. 0 for the fog flow model.

If it is recalled that there is a basic difference between the Lockhart-Martinelli correlation and the Koestel, et al. fog flow model in the determination of Φ_g, the general expression used to evaluate the incremental static-pressure change for the two correlations with an assumed velocity ratio of 1. 0 is

$$\Delta P_s = \Phi_g^2 \left(\frac{dP_g}{dL}\right) \Delta L + \frac{w_{g,in}}{g_c \bar{A}_t} \left(V_{g,i+1} - V_{g,i}\right) \tag{B32}$$

For the Lockhart-Martinelli correlation with an assumed velocity ratio of 0. 5, the static-pressure change was obtained from

$$\Delta P_s = \Phi_g^2 \left(\frac{dP_g}{dL}\right) \Delta L + \frac{w_{g,in}}{2g_c \bar{A}_t} \left[V_{g,i+1}\left(1 + x_{i+1}\right) - V_{g,i}\left(1 + x_i\right)\right] \tag{B33}$$

With an assumed velocity ratio of 0. 0, the momentum of the liquid is neglected and the expression for pressure change became

$$\Delta P_s = \Phi_g^2 \left(\frac{dP_g}{dL}\right) \Delta L + \frac{w_{g,in}}{g_c \bar{A}_t} \left(V_{g,i+1} x_{i+1} - V_{g,i} x_i\right) \tag{B34}$$

A detailed derivation of the equations is given in appendix B.

RESULTS AND DISCUSSION

The experimental data are tabulated in table II. The mercury flow and quality determination at the condenser inlet together with sets of typical condenser pressure traces are discussed briefly in appendix C.

Mercury Inlet Static-Pressure Characteristics

The mercury inlet static pressures obtained for nominal mercury and NaK flow rates of 155 and 515 pounds per hour, respectively, and a nominal NaK inlet temperature of 500° F are plotted as a function of condensing length in figure 3. The results indicate that the mercury inlet pressure became less sensitive to changes of the condensing length

TABLE II. - EXPERIMENTAL DATA

Run identification number	Inlet mercury flow rate, w_g, lb/hr	NaK flow rate, w_N, lb/hr	Condensing length, ℓ_c, in.	NaK inlet temperature, $T_{N,in}$, °F	NaK outlet temperature, $T_{N,out}$, °F	Mercury tube inlet temperature, $T_{g,in}$, °F	Mercury inlet static pressure, $P_{s,in}$, psia	Mercury static pressure 12 inches from inlet, $P_{s,12}$, psia	Mercury static pressure 25 inches from inlet, $P_{s,25}$, psia	Mercury static pressure 38 inches from inlet, $P_{s,38}$, psia	Mercury outlet static pressure, $P_{s,out}$, psia	Calculated mercury inlet quality, x
1	152	517	7	496	679	712	21.52	22.28	22.42	21.72	21.94	0.99
2	147	515	8	497	680	702	19.57	20.31	20.47	19.88	20.00	.96
3	148	516	8	496	680	700	19.24	20.02	20.11	19.61	19.70	.96
4	160	514	8	497	681	706	20.73	21.00	21.03	20.78	20.79	1.04
5	150	516	9	500	686	706	20.46	21.31	21.61	20.90	21.11	.97
6	161	514	9	496	686	702	19.55	19.86	19.92	19.56	19.74	1.05
7	149	516	10	497	687	698	18.93	19.70	19.82	19.30	19.50	.97
8	149	517	10	497	682	696	18.29	19.10	19.12	18.58	18.82	.97
9	161	515	10	496	682	696	18.45	18.78	18.80	18.61	18.59	1.05
10	153	515	10	495	685	696	18.92	19.28	19.22	19.03	19.16	1.03
11	156	514	11	504	686	698	18.73	19.60	19.88	19.30	19.55	1.02
12	154	516	11	497	687	696	18.34	19.20	19.37	18.80	19.00	1.00
13	149	515	11	498	683	691	17.34	18.70	18.30	17.72	17.98	.98
14	161	514	12	497	682	689	17.30	17.60	17.68	17.50	17.54	1.06
15	154	517	13	498	686	692	17.84	18.60	18.74	18.27	18.49	1.00
16	160	516	13	497	684	691	17.77	17.98	18.17	17.82	17.94	1.04
17	159	516	14	502	683	688	17.16	17.23	17.62	17.30	17.40	1.03
18	155	515	14	496	688	690	17.76	18.10	18.11	18.07	18.05	1.01
19	155	515	14	502	687	690	17.70	17.92	18.19	18.09	18.15	1.01
20	149	515	15	497	682	690	17.24	17.69	18.30	-----	17.84	1.02
21	156	515	15	497	683	687	17.00	16.79	17.42	17.03	17.20	1.02
22	160	516	15	496	684	687	16.90	16.80	17.40	17.26	17.19	1.04
23	157	515	15	497	684	688	17.48	17.33	17.80	17.79	17.79	1.02
24	153	515	18	498	684	687	16.97	16.83	18.17	17.62	17.66	1.00
25	152	517	19	497	687	689	17.08	16.66	18.10	17.61	17.78	1.00
26	152	517	20	498	683	686	16.59	15.99	17.59	-----	17.15	.98
27	161	516	20	503	682	684	16.63	15.68	16.90	16.87	17.04	1.05
28	162	513	20	503	687	688	17.38	16.46	17.63	17.74	17.84	1.01
29	158	515	20	502	684	687	16.91	15.90	16.99	17.24	17.33	1.03
30	153	515	21	497	686	688	17.00	16.40	18.04	17.52	17.70	1.00
31	158	513	23	503	685	686	16.82	15.72	16.76	17.01	17.13	1.03
32	153	517	24	499	684	687	16.71	15.94	17.12	17.24	17.40	1.00
33	161	515	24	502	685	686	16.70	15.52	16.49	16.95	16.90	1.04
34	158	513	24	502	685	687	17.11	16.00	16.95	17.34	17.33	1.02
35	150	517	25	499	686	687	16.99	16.25	17.30	17.50	17.54	.98
36	163	516	27	496	686	688	17.09	15.86	16.12	17.05	17.24	1.06
37	163	515	27	498	685	686	16.64	15.47	16.11	16.69	16.73	1.06
38	159	515	28	500	683	683	15.67	15.52	14.28	15.69	15.58	1.04
39	158	515	29	500	682	682	16.12	14.93	14.02	15.63	15.91	1.03
40	161	515	29	497	686	686	17.08	15.80	14.74	16.57	16.92	1.05
41	159	513	29	500	684	686	16.86	15.62	14.44	16.49	17.02	1.04
42	152	518	30	495	686	686	16.56	15.75	14.20	16.98	17.15	.99
43	159	516	32	500	685	686	17.13	15.88	13.43	16.26	16.45	1.04
44	158	515	34	498	685	686	16.92	15.62	12.81	16.92	16.88	1.03

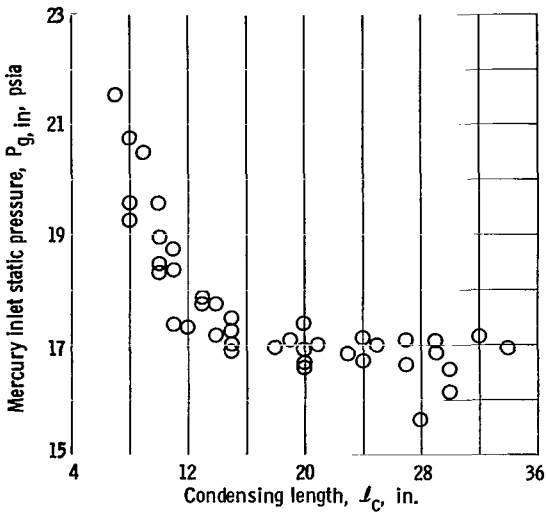

Figure 3. - Variation of mercury inlet static pressure. Nominal mercury flow rate, 155 pounds per hour; nominal NaK flow rate, 515 pounds per hour; nominal NaK inlet temperature, 498° F.

as the condensing length was increased. The mercury inlet pressure decreased sharply from 21.5 to approximately 17.0 pounds per square inch absolute as the condensing length was increased from 7 to 16 inches. As the condensing length was further increased from 16 to 34 inches, the inlet pressure decreased at a much lower rate (from ~17 to ~16.5 psia).

The trend of the mercury inlet static-pressure data can be explained by considering the heat transfer characteristics of the condensing portion of the condenser, which can be expressed in equation form as

$$Q = w_{g, in} h_{fg} = w_N \left(c_p\right)_N \left(T_{N, out} - T_{N, int}\right) \tag{1}$$

and

$$Q = UA_{ht}(LMTD) \tag{2}$$

where

$$LMTD = \frac{\left(T_{g, int} - T_{N, int}\right) - \left(T_{g, in} - T_{N, out}\right)}{\ln \left(\frac{T_{g, int} - T_{N, int}}{T_{g, in} - T_{N, out}}\right)} \tag{3}$$

The mercury flow rate and inlet quality were maintained approximately constant for various condensing lengths resulting in a constant heat load Q. The overall unit conductance U and the mercury vapor temperature can be assumed constant along the tube to simplify the discussion (ref. 7). The heat transfer area, therefore, varied inversely with the LMTD, as shown by equation (2); in other words, as condensing length was increased, the log mean temperature difference between the mercury and the NaK had to decrease.

By employing the assumption that the mercury vapor saturation temperature does not vary along the tube, the LMTD can be rearranged to

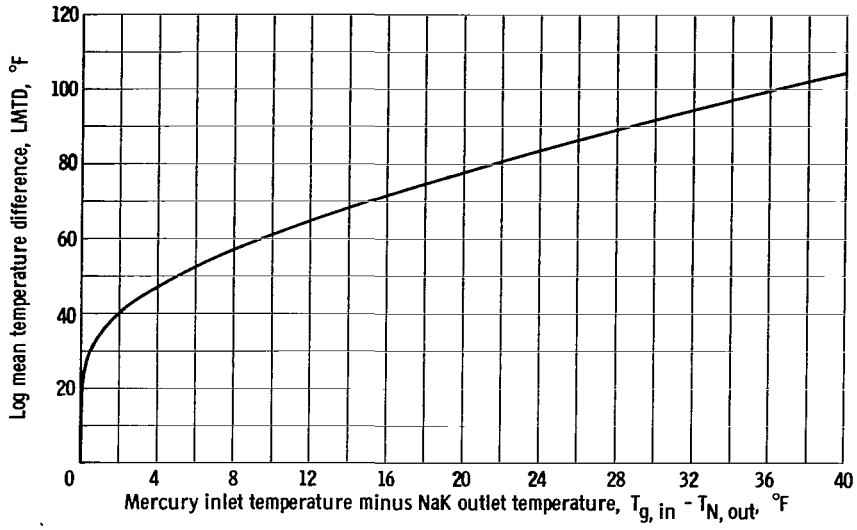

Figure 4. - Relation between log mean temperature difference and mercury inlet temperature minus NaK outlet temperature. NaK temperature difference, 175° F.

$$LMTD = \frac{\Delta T_N}{\ln\left(1 + \frac{\Delta T_N}{T_{g, in} - T_{N, out}}\right)} \tag{4}$$

Because the heat load and NaK flow rate were held constant, within experimental limits, the NaK temperature rise across the condensing portion of the tube remained about constant at 175° F. The LMTD then becomes a function of the temperature difference $T_{g, in} - T_{N, out}$ as shown by equation (4). The relation between the LMTD and $T_{g, in} - T_{N, out}$, presented in figure 4 for $\Delta T_N = 175^{\circ}$ F, shows that the temperature difference $T_{g, in} - T_{N, out}$ becomes less sensitive to changes of the LMTD as the LMTD decreases. Therefore, it would be expected that the temperature difference $T_{g, in} - T_{N, out}$ becomes less sensitive to condensing length as the condensing length, hence heat transfer area, is increased.

The experimental temperature difference between the mercury inlet and NaK outlet is shown as a function of condensing length in figure 5. As the condensing length was increased from 7 to 16 inches, the temperature difference was reduced from 33° to 3° F. A further increase of condensing length, beyond 16 inches, reduced the temperature difference below 3° F, resulting in the required variation of LMTD as the condensing length was increased from 16 to 34 inches. Because the LMTD was small for the longer condensing lengths, the LMTD was highly sensitive to small changes of $T_{g, in} - T_{N, out}$.

It should be noted from figures 3 and 5 that the trend of the temperature difference data is similar to the trend of the mercury inlet static-pressure data and can be explained by the fact that during the experimental tests the mercury vapor flow rate, the NaK flow rate, and the NaK inlet temperature were held constant, within experimental limits, for

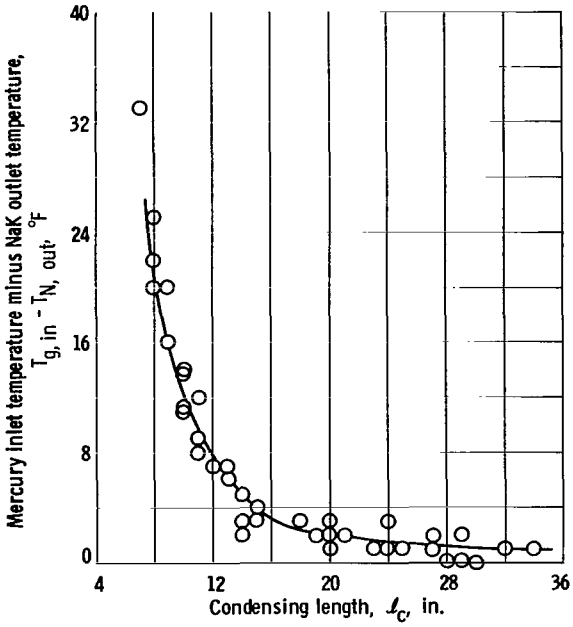

Figure 5. - Mercury inlet temperature minus NaK outlet temperature as function of condensing length. Nominal mercury flow rate, 155 pounds per hour; nominal NaK flow rate, 515 pounds per hour; nominal NaK inlet temperature, 498° F.

the various condensing lengths. Since the total heat rejected was constant, the NaK outlet temperature remained approximately constant and the change of $T_{g, in} - T_{N, out}$, required as the condensing length was varied, resulted from a change of mercury inlet temperature. The mercury inlet temperature consistently agreed with the saturation temperature for the respective inlet pressure indicating no superheat existed. Therefore, as the condensing length was increased, the mercury inlet saturation temperature was reduced with a corresponding reduction of inlet static pressure.

The spread of mercury inlet pressure data resulted from minor variations of NaK outlet temperature, caused by small variations of mercury flow rate and/or NaK outlet temperature, which in turn affected the mercury inlet temperature and pressure. The fact that the minor variation of NaK outlet temperature did cause some scatter of inlet pressure data emphasizes an important consideration; the mercury inlet saturation temperature and pressure were related directly to the NaK outlet temperature.

Predicted Local Static Pressures

In addition to examining the inlet static-pressure characteristics, local static-pressure variations along the condenser were calculated and compared to the measured pressures. This study included (1) examination of the effects of the different assumed liquid-to-vapor velocity ratios and the predicted two-phase friction pressure losses on the calculated static-pressure distribution and (2) a comparison of the local static-pressure measurements with the predicted static-pressure profiles. Six representative data runs were chosen for comparison with the predicted pressure profile results as a function of condensing length. A brief discussion of the NaK temperature profile begins the discussion.

The NaK temperature profiles for three of the six representative runs (condensing lengths of 10, 20, and 34 in.) are shown in figure 6. By using the NaK shell temperatures as a guide, curves were drawn through the averages of the local NaK stream temperatures

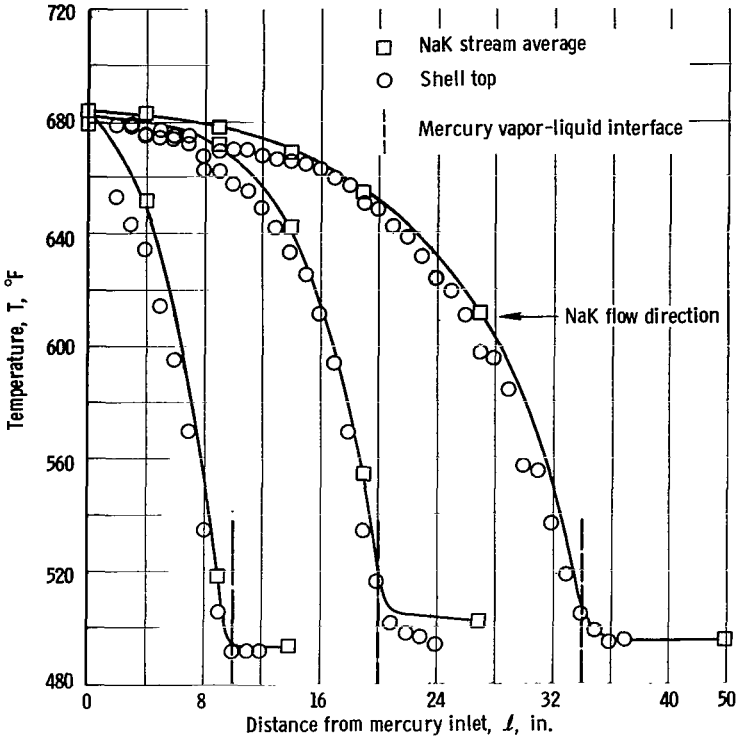

Figure 6. - NaK temperature profiles.

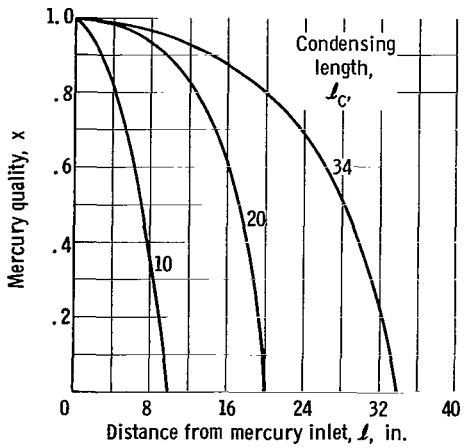

Figure 7. - Mercury quality profiles.

to obtain the NaK stream temperature profile. The temperatures used to calculate local mercury vapor qualities were taken from these NaK stream temperature profiles.

The vapor quality profiles for the three condensing lengths are shown in figure 7. Since the slope of the NaK stream temperature profile is indicative of the rate at which the thermal energy was removed from the mercury vapor, the shape of the quality distribution was the same as the temperature profile.

The predicted local vapor velocities were obtained from the local qualities (from the profiles shown in fig. 7) in conjunction with the respective local gas flow area, the measured total mercury flow rate, and the specific volume of the vapor at the predicted local saturation pressure.

Momentum and two-phase friction. - The predicted axial vapor velocity profiles, the predicted pressure changes due to momentum changes, and the predicted two-phase frictional pressure losses are presented in figures 8, 9, and 10 for condensing lengths of 10, 20, and 34 inches, respectively.

The predicted vapor velocity profiles are shown in figures 8(a), 9(a), and 10(a). For the 10-inch condensing length, the decrease of quality was greater, on a percentage basis, than the decrease of the flow area for the tapered tube. Therefore, the predicted vapor velocity decreased for the entire vapor length.

In the initial portions of the vapor lengths for the 20- and 34-inch condensing lengths the vapor velocities increased; initially, the quality decrease for the increments was less, on a percentage basis, than the decrease of flow area. This situation was reversed in the last half of the condensing length, and the predicted vapor velocities then decreased.

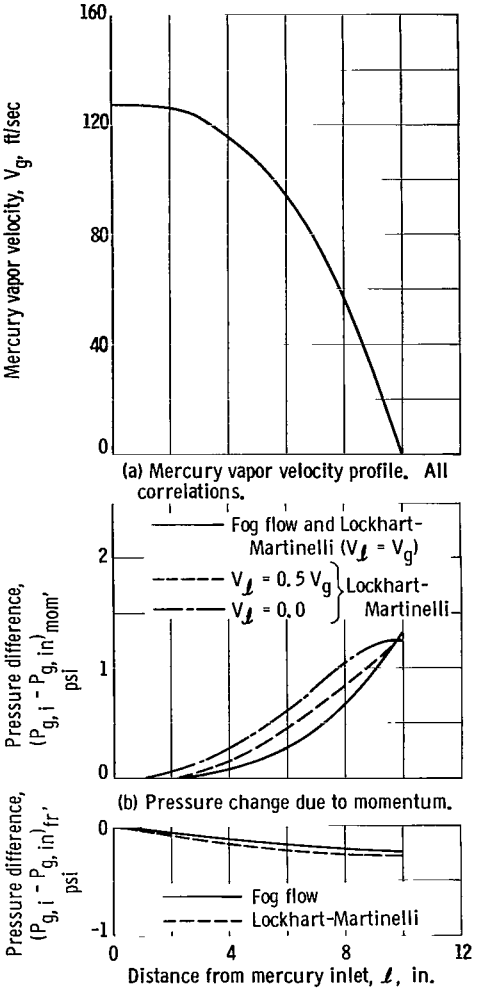

(a) Mercury vapor velocity profile. All correlations.

(b) Pressure change due to momentum.

(c) Frictional pressure loss.

Figure 8. - Mercury vapor velocity profiles and pressure profiles due to momentum changes and friction. Run 10; mercury flow rate, 153 pounds per hour; NaK flow rate, 515 pounds per hour.

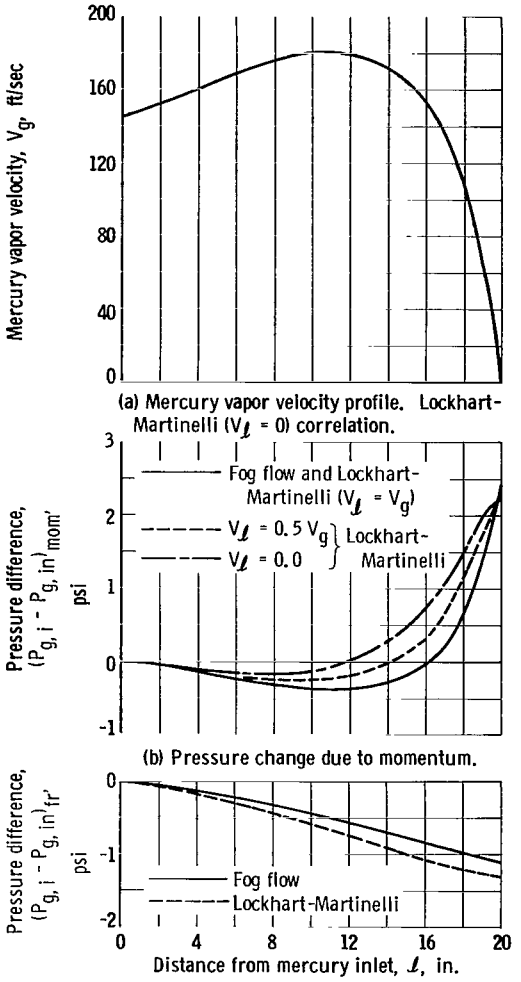

(a) Mercury vapor velocity profile. Lockhart-Martinelli ($V_\ell = 0$) correlation.

(b) Pressure change due to momentum.

(c) Frictional pressure loss.

Figure 9. - Mercury vapor velocity profile and pressure profiles due to momentum changes and friction. Run 28; mercury flow rate, 162 pounds per hour; NaK flow rate, 513 pounds per hour.

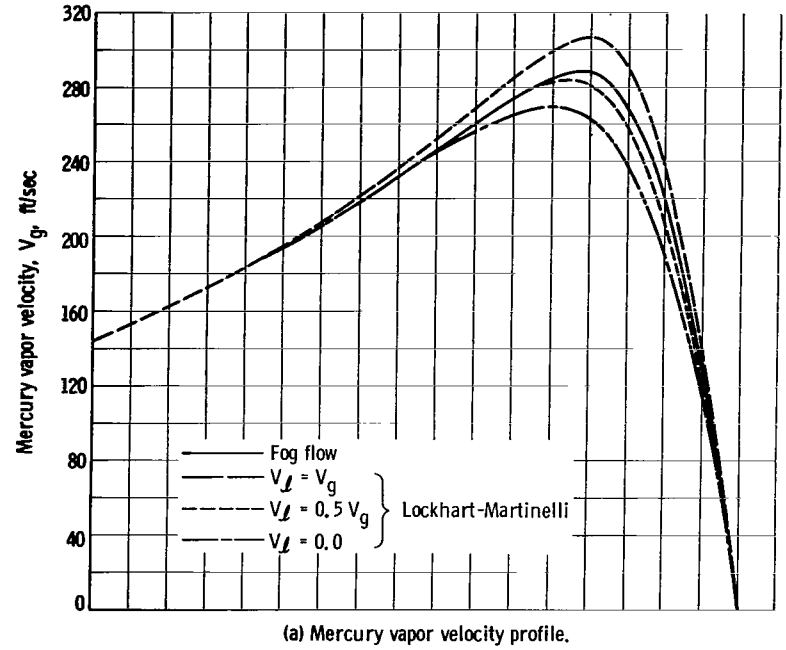

(a) Mercury vapor velocity profile.

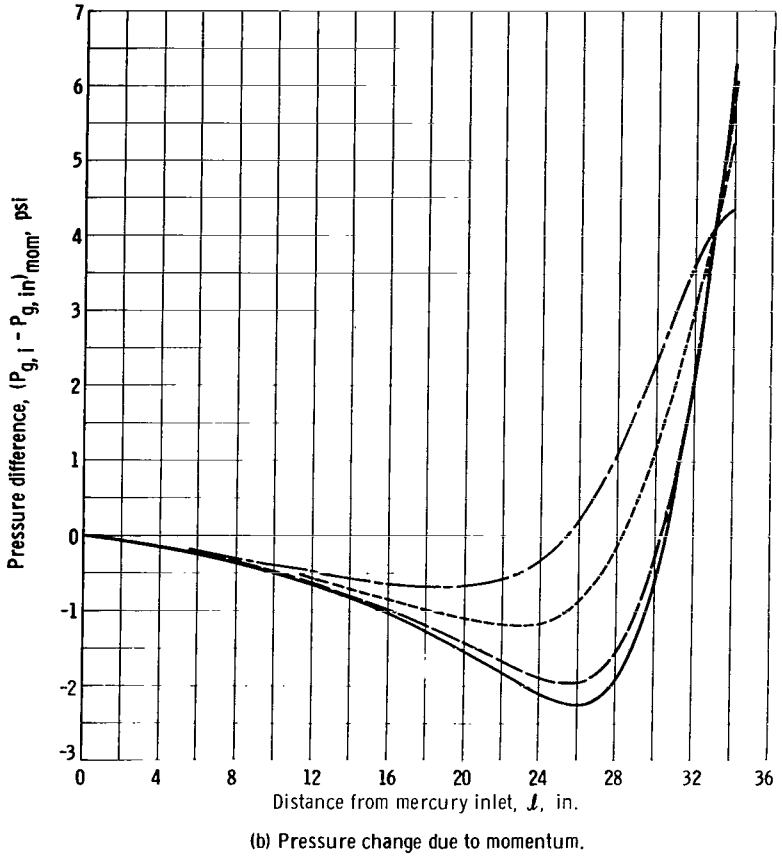

(b) Pressure change due to momentum.

Figure 10. - Mercury vapor velocity profile and pressure profiles due to momentum changes and friction. Run 44; mercury flow rate, 158 pounds per hour; NaK flow rate, 515 pounds per hour.

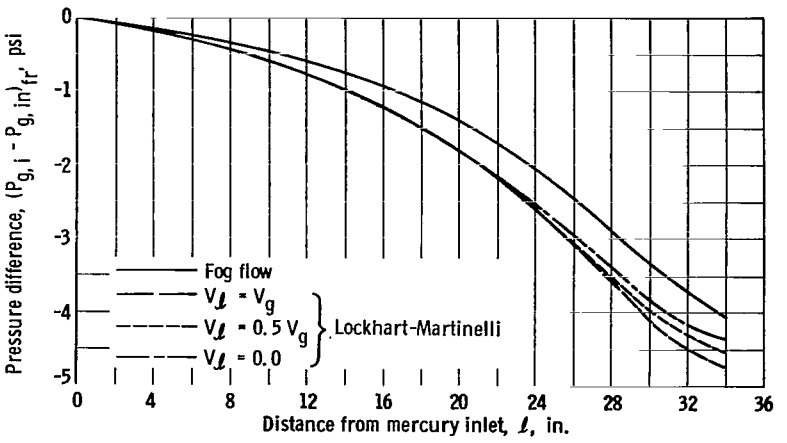

(c) Frictional pressure loss.

Figure 10. - Concluded.

The four methods of calculation produced significantly different velocity profiles for the longer condensing lengths. It is important to recall that the vapor specific volume for any increment was obtained from the pressure predicted at the beginning of the increment, except the first one, where the measured inlet static pressure was used. For the shorter condensing lengths (less than 20 in.), the differences between the static pressures predicted by the four methods were relatively small. However, the predicted static pressures for the longer condenser lengths were significantly different; thus, the four methods used significantly different vapor specific volumes. The different vapor specific volumes, then, caused the differences in predicted vapor velocity profiles for the longer condensing lengths.

There was no significant difference in the predicted vapor velocity profiles for the 10-inch condensing length. The vapor velocity shown for the 20-inch condensing length (fig. 9(a)) was determined by the Lockhart-Martinelli correlation with $V_\ell = 0.0$; the other three profiles deviated less than 3 percent from the one presented. All four velocity profiles are presented for the 34-inch condensing length (fig. 10(a)).

The predicted pressure changes due to momentum changes are presented in figures 8(b), 9(b), and 10(b). The effect of the liquid-to-vapor velocity ratio can be ascertained by comparing the three profiles obtained from the Lockhart-Martinelli correlation which was used with the three velocity ratios of 0.0, 0.5, and 1.0. Consider first the initial portions of the vapor lengths for the 20- and 34-inch condensing lengths where the vapor velocity increased. When the liquid velocity was neglected ($V_\ell/V_g = 0$), it was assumed that no energy was necessary to accelerate the liquid in the vapor stream or on the tube wall. As the liquid-to-vapor velocity ratio was increased, more energy was assumed necessary to accelerate both the liquid in the vapor stream and the liquid on the wall to an assumed velocity. Consequently, the static-pressure decrease resulting from momentum changes was largest when the liquid-to-vapor velocity ratio was 1.0.

Consider next, the effect of velocity ratio in the portions of the vapor length where the vapor velocity decreased. This included the entire vapor length for the 10-inch condensing length. When the liquid velocity was neglected, the predicted pressure increase resulted solely from the velocity decrease of the vapor phase. As the assumed liquid-to-vapor velocity ratio was increased, the vapor momentum changes predicted by the three methods remained about constant because the different velocity profiles did not significantly affect the momentum changes; however, the predicted momentum change of the liquid then contributed significantly to the pressure rise. Therefore, in the portions of the vapor length where the vapor velocity decreased, the predicted pressure recovery was largest when the liquid velocity was assumed to be equal to the vapor velocity.

After examining the effects of momentum changes on the predicted static pressures, the two-phase frictional pressure losses will be defined for various flow conditions. The predicted two-phase frictional pressure losses are presented in figures 8(c), 9(c), and 10(c). To determine the differences between the two methods used to evaluate the parameter Φ_g, the effect of velocity ratio should be eliminated. The velocity ratio effect can be eliminated by comparing the two-phase frictional losses predicted by the Lockhart-Martinelli correlation used with a liquid-to-vapor velocity ratio of 1.0, to losses predicted by the fog flow model (where $V_\ell/V_g = 1.0$, also). The Lockhart-Martinelli correlation, with $V_\ell = V_g$, predicted a larger value for the two-phase friction parameter Φ_g than the fog flow model for all increments except the last one or two. As a result, the two-phase frictional pressure losses predicted by the Lockhart-Martinelli correlation used with a velocity ratio of 1.0, were larger than the losses predicted by the fog flow model for all increments but the last one or two.

Comparison of data and local predicted pressures. - Typical predicted static-pressure profiles along with measured static pressures are presented in figure 11 (see pp. 19-20). The calculated static-pressure profiles include the effects of the predicted momentum change and two-phase friction for each case. The effects of the different liquid-to-vapor velocity ratios on static-pressure distribution are clearly seen by comparing the three profiles obtained from the Lockhart-Martinelli correlation with each other. The effects of the different two-phase friction parameter Φ_g on the static-pressure distribution are seen by comparing the distributions of the Lockhart-Martinelli correlation, when the liquid-to-vapor velocity was assumed to be 1.0, with the results of the Koestel, et al. fog flow model.

The pressures that were predicted when the liquid-to-vapor velocity ratio was 0.5 for the Lockhart-Martinelli correlation and 1.0 for both correlations agreed best with the pressures measured in the initial 75 percent of the vapor length. However, the predicted static pressures were higher than the static pressures measured in the last 25 percent of the vapor length. The static pressures predicted in the final portion of the condensing length could be reduced by either of two means; the velocity ratio could

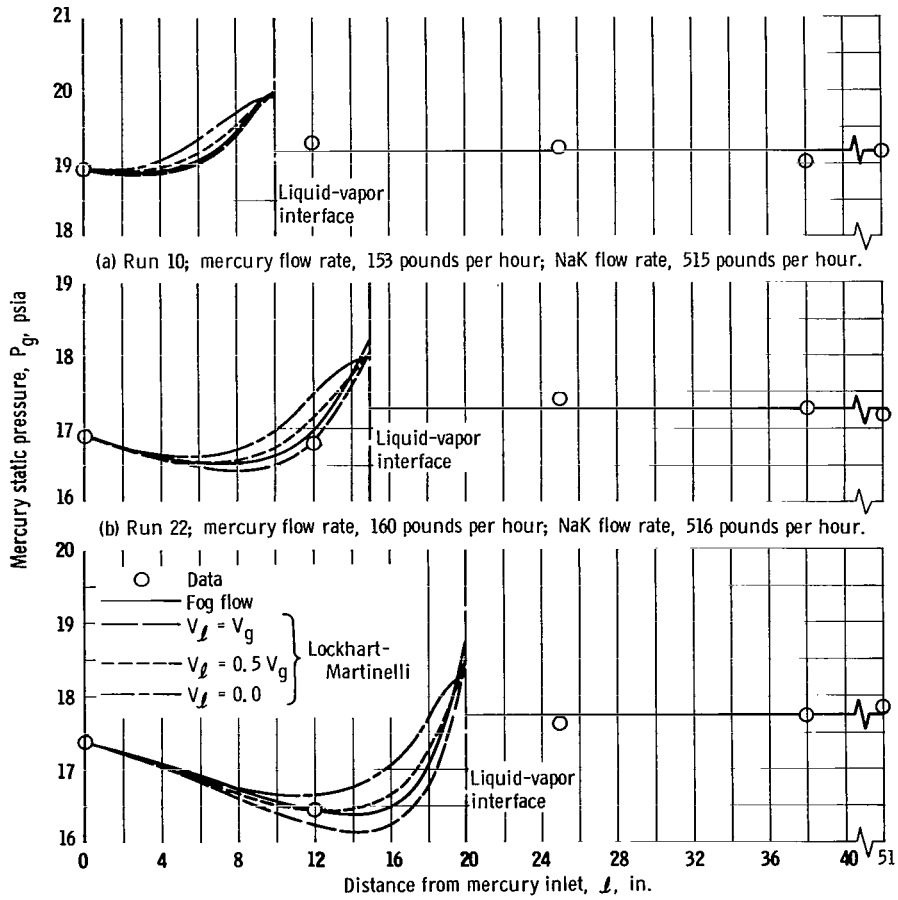

(a) Run 10; mercury flow rate, 153 pounds per hour; NaK flow rate, 515 pounds per hour.

(b) Run 22; mercury flow rate, 160 pounds per hour; NaK flow rate, 516 pounds per hour.

(c) Run 28; mercury flow rate, 162 pounds per hour; NaK flow rate, 513 pounds per hour.

Figure 11. - Comparison of predicted profiles with data.

be reduced in that portion to reduce pressure recovery, or the two-phase friction parameter Φ_g could be increased to increase the frictional pressure losses.

Other investigators (refs. 2 and 4) have indicated that an increased liquid-to-vapor velocity ratio exists in the final portion of the vapor length because of liquid inertia. If the possibility of a reduced velocity ratio is eliminated, an increased friction parameter Φ_g is then indicated in the final portions of the vapor length where the quality is less than 40 percent for both friction correlations. Other investigators (refs. 5 and 8) have reported experimental friction factors Φ_g that were larger than the predicted factors in the low quality portions of the vapor length.

The best agreement between the pressures calculated at the liquid-vapor interface and the pressures measured in the condensate was obtained for the Lockhart-Martinelli correlation with $V_\ell/V_g = 0.0$. When the effects of the liquid momentum were neglected, however, the calculated pressure profiles did not agree well with the pressures measured in the vapor.

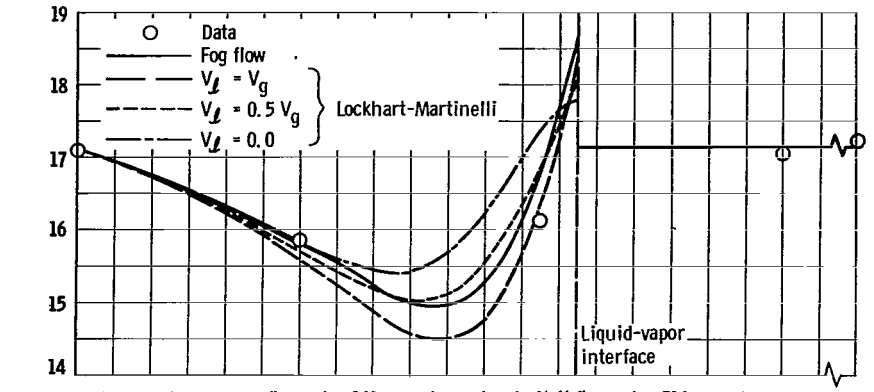

(d) Run 36; mercury flow rate, 163 pounds per hour; NaK flow rate, 516 pounds per hour.

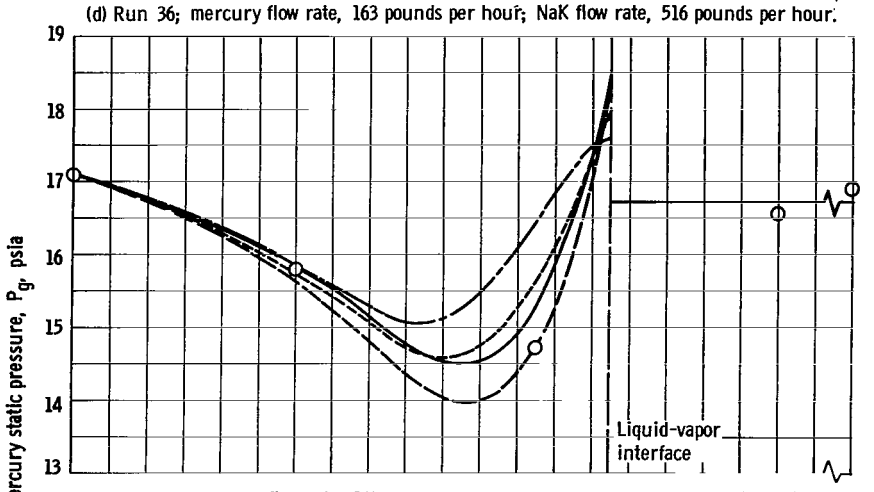

(e) Run 40; mercury flow rate, 161 pounds per hour; NaK flow rate, 515 pounds per hour.

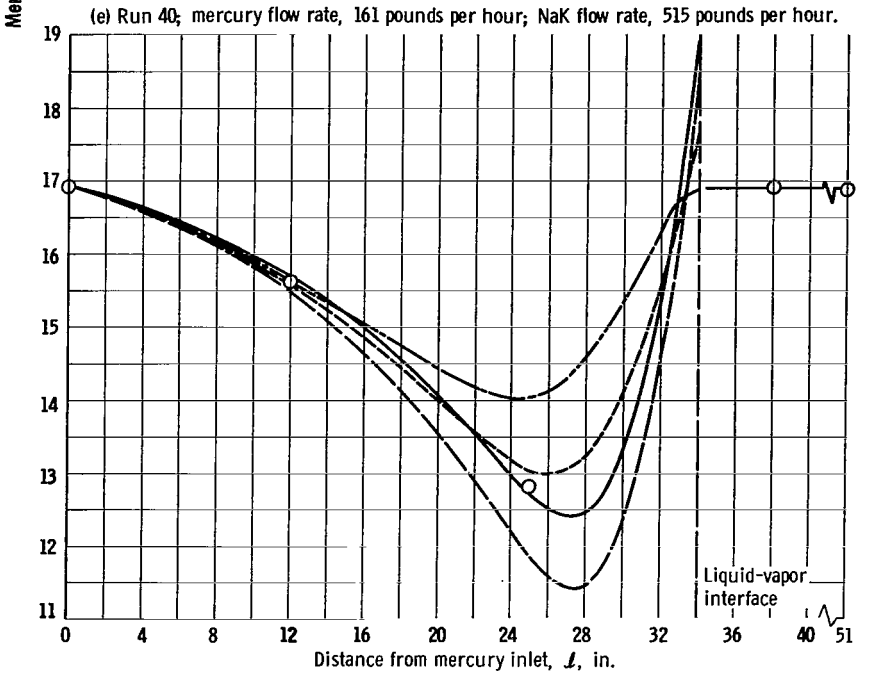

(f) Run 44; mercury flow rate, 158 pounds per hour; NaK flow rate, 515 pounds per hour.

Figure 11. - Concluded.

Overall Pressure Difference

After the predicted local static pressures have been compared with the local measured pressures, the experimental and predicted overall pressure differences are presented in figure 12. The overall pressure difference was obtained from the experimental data by subtracting the average of the static pressures measured in the liquid leg from the measured inlet static pressure. The data show a small pressure rise, about 0.5 pound per square inch, for condensing lengths of less than 20 inches. The pressure rise decreased as condensing length was increased such that a pressure drop of about 0.5 pound per square inch occurred at a condensing length of 34 inches.

The effect of the different two-phase friction parameter Φ_g on the overall pressure difference is seen by comparing the results of the Lockhart-Martinelli correlation, obtained with $V_\ell = V_g$, to the results of the Koestel, et al. fog flow model. The net pressure changes for these two cases where $V_\ell = V_g$ was assumed indicated an increase in pressure rise with an increase in condensing length; the pressure rise due to momentum changes increased faster than the predicted two-phase frictional pressure losses. The effect of varying the liquid-to-vapor velocity ratio on the overall pressure difference is seen by comparing the results obtained from the three assumed velocity ratios used with the Lockhart-Martinelli correlation.

The overall pressure difference obtained from the Lockhart-Martinelli correlation used with an assumed velocity ratio of 0.0 agreed best with the pressure difference obtained from the experimental data. None of the four methods of calculation was considered satisfactory for predicting both the local pressures and the overall pressure differences.

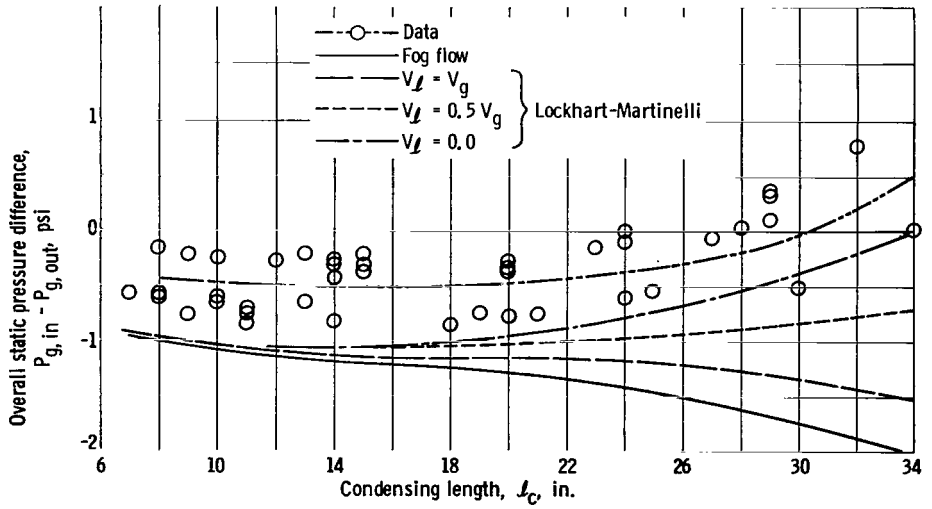

Figure 12. - Overall pressure difference as function of condensing length. Nominal mercury flow rate, 155 pounds per hour; nominal NaK flow rate, 515 pounds per hour; nominal NaK inlet temperature, 498° F.

SUMMARY OF RESULTS

This investigation was initiated to define such pressure characteristics as the relation between inlet static pressure and condensing length and the overall pressure change as a function of condensing length for the nonwetting flow of mercury, condensing in a NaK-cooled, counterflow, tapered tube heat exchanger. Four methods of predicting static pressures for condensing flow, the correlation of Lockhart and Martinelli used with liquid-to-vapor velocity ratios of 0.0, 0.5, and 1.0, and the fog flow model of Koestel, et al. used with a liquid-to-vapor velocity ratio of 1.0, were compared to the measured static pressures. The results can be summarized as follows:

1. The mercury inlet static pressure exhibited a high sensitivity to changes of condensing length for short condensing lengths, less than 16 inches, and became much less sensitive as the condensing length was increased. The inlet pressure decreased sharply from 21.5 to approximately 17 pounds per square inch absolute as the condensing length was increased from 7 to 16 inches and decreased much more gradually, from 17 to about 16.5 pounds per square inch absolute, as the condensing length was further increased from 16 to 34 inches. Because the mercury inlet saturation temperature and pressure were related directly to the NaK outlet temperature, small variations in NaK outlet temperature resulted in small variations of mercury inlet temperature and pressure.

2. The experimental pressure difference for the condensing length varied from a small pressure rise, about 0.5 pound per square inch, which occurred for condensing lengths of less than 20 inches to a small pressure drop, about 0.5 pound per square inch, which occurred at a condensing length of 34 inches. Generally, both the Lockhart-Martinelli correlation and the fog flow model of Koestel, et al. produced net pressure changes for the condensing length that indicated more pressure rise than the data showed. The case using the Lockhart-Martinelli correlation with a liquid-to-vapor velocity ratio of 0.0 produced net pressure changes that agreed best with the data.

3. The Lockhart-Martinelli correlation resulted in static-pressure profiles that generally agreed with the static pressures measured in the initial 75 percent of the vapor length when the assumed liquid-to-vapor velocity ratio was both 0.5 and 1.0. Generally the Lockhart-Martinelli correlation produced results that did not agree well with the local measured static pressures when the momentum effects of the liquid were neglected. The two-phase friction parameter Φ_g predicted by the Lockhart-Martinelli correlation appeared to be low in the final 25 percent of the vapor length.

4. The Koestel, et al. fog flow model, wherein the liquid-to-vapor velocity ratio was assumed to be 1.0, resulted in pressure profiles that generally agreed with the measured pressures in the first 75 percent of the condensing length. The two-phase friction param-

eter Φ_g predicted by the Koestel, et al. model appeared to be low in the last 25 percent of the condensing length.

Lewis Research Center,
National Aeronautics and Space Administration,
Cleveland, Ohio, July 20, 1966,
701-04-00-02-22.

APPENDIX A

SYMBOLS

A_g	mercury vapor flow area
A_{ht}	heat transfer area
A_t	tube cross-sectional area
$\bar{A}_t$	mean tube cross-sectional area for increment
c_p	specific heat
D	tube inside diameter
D_m	diameter of flow passage formed by condensed drops on tube wall
f	friction factor
f	function of
g_c	conversion factor
h_{fg}	mercury latent heat of vaporization
L	length
LMTD	log mean temperature difference
ℓ	distance from mercury inlet
ℓ_c	condensing length
P	pressure
Q	heat transfer rate
Re	Reynolds number
T	temperature
U	overall heat transfer coefficient
V	velocity
v	specific volume
We	Weber number
w	flow rate
x	quality
Δ	finite difference
μ	viscosity
ρ	density
σ	surface tension of liquid mercury
Φ_g	Lockhart-Martinelli parameter
χ	two-phase flow molulus $\sqrt{(\Delta P/\Delta L)_\ell/(\Delta P/\Delta L)_g}$

Subscripts:

fr	friction
g	mercury vapor
i	any section along tube
i+1	section 1-inch downstream from section i
in	inlet
int	mercury interface
ℓ	liquid mercury
mom	momentum
N	NaK
out	outlet
s	static
TPF	two-phase friction
tt	turbulent liquid, turbulent gas
vt	viscous liquid, turbulent gas

APPENDIX B

DERIVATION OF EQUATIONS

When the drag forces due to liquid droplets are neglected, the static-pressure change for two-phase flow in a tube for a finite incremental length can be expressed as

$$\Delta P_s = \Delta P_{TPF} + \Delta P_{mom} \tag{B1}$$

The correlations of Lockhart-Martinelli and Koestel, et al. were used to calculate the two-phase frictional pressure changes. Lockhart and Martinelli express the two-phase frictional pressure gradient as a function of the parameter Φ_g and the frictional pressure gradient of the vapor determined as if the vapor flowed alone in the tube; that is,

$$\frac{dP_{TPF}}{dL} = \Phi_g^2 \left(\frac{dP_g}{dL}\right) \tag{B2}$$

For the 1-inch increments, the two-phase frictional pressure change could be written as

$$\Delta P_{TPF} = \Phi_g^2 \left(\frac{dP_g}{dL}\right) \Delta L \tag{B3}$$

The parameter Φ_g is a function of the parameter χ for the Lockhart-Martinelli correlation. The value of χ depends upon the superficial Reynolds numbers of the liquid and gas phases. The superficial Reynolds numbers were evaluated by assuming a single phase flowed alone in the tube. For Reynolds numbers less than 2000 the flow for the phase was assumed to be viscous, and for values greater than 2000 the flow was assumed to be turbulent. When the liquid and vapor phase Reynolds numbers were greater than 2000, a turbulent liquid-turbulent vapor flow condition was assumed and χ was evaluated from

$$\chi_{tt} = \left(\frac{1 - x}{x}\right)^{0.9} \left(\frac{v_\ell}{v_g}\right)^{0.5} \left(\frac{\mu_\ell}{\mu_g}\right)^{0.1} \tag{B4}$$

When a viscous liquid-turbulent vapor flow condition existed (i.e., $Re_\ell < 2000$, $Re_g > 2000$), χ was determined from the following equation:

$$\chi_{vt} = \left(\frac{16.0}{0.046}\right)^{0.5}\left(\frac{v_\ell}{v_g}\right)^{0.5}\left(\frac{\mu_\ell}{\mu_g}\right)^{0.5}\left(\frac{1-x}{x}\right)^{0.5}\frac{1}{Re_g^{0.4}} \tag{B5}$$

The mercury vapor quality at any section within the condensing length, obtained from heat balance ratios, can be expressed as

$$x_i = x_{in}\left(1 - \frac{T_{N,out} - T_{N,i}}{T_{N,out} - T_{N,int}}\right) \tag{B6}$$

Because the vapor phase Reynolds numbers were always greater than 2000, the frictional pressure gradient for this phase was evaluated by using the Fanning equation, that is,

$$\frac{dP_g}{dL} = \frac{2.0\, f V_g^2}{D v_g g_c} \tag{B7}$$

where the following friction factor of the Blasius form for turbulent flow in a smooth tube was assumed (ref. 9):

$$f = \frac{0.046}{Re_g^{0.2}} \tag{B8}$$

The velocity of the vapor at any section was determined from

$$V_{g,i} = \frac{w_{g,in} v_{g,i} x_i}{A_{g,i}} \tag{B9}$$

where

$$A_{g,i} = \frac{A_{t,i}}{1.0 + \frac{v_{\ell,i}}{v_{g,i}}\left(\frac{1-x_i}{x_i}\right)} \tag{B10}$$

In the fog flow model correlation (ref. 3), the two-phase frictional pressure gradient is expressed as

$$\frac{dP_{TPF}}{dL} = \Phi_g^2 \frac{dP_g}{dL} \tag{B11}$$

where the parameter Φ_g is given as a function of the vapor quality and the Weber number based on the tube diameter, that is,

$$\Phi_g^2 x^{3/4} = f(We) = f\left(\frac{DV_g^2}{2v_g g_c \sigma}\right) \tag{B12}$$

The Weber number is shown to be a function of the ratio of the tube diameter to the diameter of the fog flow passage by the following equation:

$$We = \frac{0.3712}{\left(\frac{D}{D_m}\right)^{4.0} - \left(\frac{D}{D_m}\right)^{3.0}} \tag{B13}$$

The quantity $\Phi_g^2 x^{3/4}$ is also shown to be a function of the diameter ratio; that is,

$$\Phi_g^2 x^{3/4} = \left(\frac{D}{D_m}\right)^{4.75} \tag{B14}$$

To obtain the relation between $\Phi_g^2 x^{3/4}$ and the Weber number, values of D/D_m were assumed and equations (B13) and (B14) were solved for the respective values of $\Phi_g^2 x^{3/4}$ and the Weber number. Knowing the relation between $\Phi_g^2 x^{3/4}$ and the Weber number plus the quality at any section makes it possible to solve for Φ_g for each increment. The vapor phase frictional pressure gradient dP_g/dL for the fog flow model was evaluated by the same method employed for the Lockhart-Martinelli correlation.

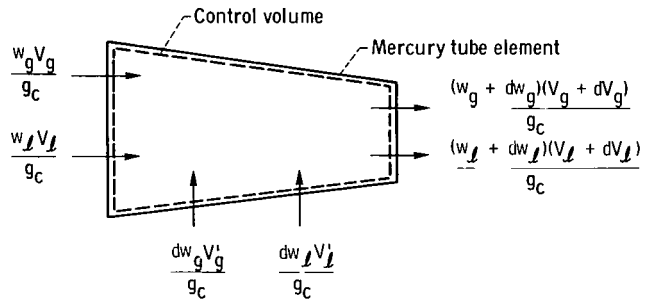

Figure 13. - Liquid and vapor momentum terms.

After the incremental two-phase frictional pressure change was determined, the pressure change due to momentum changes was required. Referring to figure 13 reveals that, for small changes in cross-sectional area for the increment, the pressure change due to the momentum changes for the two phases is

$$\Delta P_{mom} = \frac{1}{g_c \bar{A}_t} \left[\left(w_g + dw_g\right)\left(V_g + dV_g\right) + \left(w_\ell + dw_\ell\right)\left(V_\ell + dV_\ell\right) \right.$$

$$\left. - dw_g V'_g - dw_\ell V'_\ell - w_g V_g - w_\ell V_\ell \right] \qquad \text{(B15)}$$

where

$$\bar{A}_t = \frac{A_{t,i} + A_{t,i+1}}{2}$$

The term V'_g represents the velocity of the vapor that is condensed within the increment just before condensation occurs. The term V'_ℓ represents the velocity of the liquid droplets entrained into the vapor stream just before entrainment occurs. The vapor condensed in the increment was assumed to have a velocity equal to zero just before condensation occurred. The liquid droplets were assumed to be at rest on the wall before being entrained into the vapor stream. Therefore, both V'_g and V'_ℓ were assumed to be zero in equation (B15). These assumptions yielded the following:

$$\Delta P_{mom} = \frac{1}{g_c \bar{A}_t} \left[\left(w_g + dw_g\right)\left(V_g + dV_g\right) + \left(w_\ell + dw_\ell\right)\left(V_\ell + dV_\ell\right) - w_g V_g - w_\ell V_\ell \right] \qquad \text{(B16)}$$

Both the vapor velocity V_g and the liquid velocity V_ℓ are needed to evaluate equation (B16). The vapor velocity was obtained from equation (B9); then the liquid velocity was obtained by assuming the three liquid-to-vapor velocity ratios of 1.0, 0.5, and 0.0 for the Lockhart-Martinelli correlation. For the fog flow model a liquid-to-vapor velocity ratio of 1.0 was assumed, (ref. 2).

Because steady flow through the increment existed, the total flow rate remained constant and the decrease in vapor flow rate equalled the increase in liquid flow rate; that is,

$$-dw_g = dw_\ell \qquad \text{(B17)}$$

When a liquid-to-vapor velocity of 1.0 was assumed, then

$$V_\ell = V_g \qquad \text{(B18)}$$

$$dV_\ell = dV_g \qquad \text{(B19)}$$

Substituting equations (B17) to (B19) into equation (B16) yields the pressure change due to momentum changes for a liquid-to-vapor velocity ratio of 1.0, which is

$$\Delta P_{mom} = \frac{1}{g_c \bar{A}_t} \left[\left(w_g + dw_g \right) dV_g + \left(w_\ell + dw_\ell \right) dV_g \right] \tag{B20}$$

When the liquid-to-vapor velocity ratio of 0. 5 is assumed, the relation between the liquid and vapor velocities becomes

$$V_\ell = 0.5\, V_g \tag{B21}$$

$$dV_\ell = 0.5\, dV_g \tag{B22}$$

Substituting equations (B17), (B21), and (B22) into equation (B16) yields

$$\Delta P_{mom} = \frac{1}{g_c \bar{A}_t} \left[\left(w_g + dw_g \right) dV_g + \left(w_\ell + dw_\ell \right) \left(0.5\, dV_g \right) + dw_g\, V_g + dw_\ell \left(0.5\, V_g \right) \right] \tag{B23}$$

The velocity of the liquid is neglected for an assumed velocity ratio of 0. 0, and equation (B16) then becomes

$$\Delta P_{mom} = \frac{1}{g_c \bar{A}_t} \left[\left(w_g + dw_g \right) dV_g + dw_g\, V_g \right] \tag{B24}$$

The mercury vapor flow rate can be expressed as a function of the total flow rate and quality at any section in the following way:

$$w_{g,\,i} = w_{g,\,in} x_i \tag{B25}$$

while the liquid mercury flow rate can be determined at any section from the following equation:

$$w_{\ell,\,i} = w_{g,\,in} - w_{g,\,i} \tag{B26}$$

The differentials dw_g and dV_g could be evaluated as finite differences from

$$\Delta w_g = w_{g,\,in} \left(x_{i+1} - x_i \right) \tag{B27}$$

and

$$\Delta V_g = w_{g,in} v_g \left(\frac{x_{i+1}}{A_{g,i+1}} - \frac{x_i}{A_{g,i}} \right) \tag{B28}$$

Substituting equation (B17) and equations (B25) to (B28) into equations (B20), (B23), and (B24) yields

$$\Delta P_{mom} = \frac{w_{g,in}}{g_c \bar{A}_t} \left(V_{g,i+1} - V_{g,i} \right) \quad \text{for } \frac{V_\ell}{V_g} = 1.0 \tag{B29}$$

$$\Delta P_{mom} = \frac{w_{g,in}}{2 g_c \bar{A}_t} \left[V_{g,i+1} \left(1 + x_{i+1} \right) - V_{g,i} \left(1 + x_i \right) \right] \quad \text{for } \frac{V_\ell}{V_g} = 0.5 \tag{B30}$$

$$\Delta P_{mom} = \frac{w_{g,in}}{g_c \bar{A}_t} \left(V_{g,i+1} x_{i+1} - V_{g,i} x_i \right) \quad \text{for } \frac{V_\ell}{V_g} = 0.0 \tag{B31}$$

respectively, which are used to evaluate the pressure change due to momentum changes for the three previously mentioned liquid-to-vapor velocity ratios. The basic difference between the Lockhart-Martinelli correlation and the Koestel, et al. fog flow model in the determination of Φ_g should be remembered. Then, for an assumed velocity ratio of 1.0 the static-pressure change for the two correlations was determined from

$$\Delta P_s = \Phi_g^2 \left(\frac{dP_g}{dL} \right) \Delta L + \frac{w_{g,in}}{g_c \bar{A}_t} \left(V_{g,i+1} - V_{g,i} \right) \tag{B32}$$

For the Lockhart-Martinelli correlation used with an assumed velocity ratio of 0.5, the static-pressure change for an increment was obtained from

$$\Delta P_s = \Phi_g^2 \left(\frac{dP_g}{dL} \right) \Delta L + \frac{w_{g,in}}{2 g_c \bar{A}_t} \left[V_{g,i+1} \left(1 + x_{i+1} \right) - V_{g,i} \left(1 + x_i \right) \right] \tag{B33}$$

When the velocity of the liquid was neglected ($V_\ell / V_g = 0.0$), the static-pressure change was determined from

$$\Delta P_s = \Phi_g^2 \left(\frac{dP_g}{dL} \right) \Delta L + \frac{w_{g,in}}{g_c \bar{A}_t} \left(V_{g,i+1} x_{i+1} - V_{g,i} x_i \right) \tag{B34}$$

APPENDIX C

TEST SECTION FLOW, QUALITY, AND PRESSURE TRACES

The vapor flow rate was calculated from the standard equation for compressible flow through a venturi (ref. 10)

$$w_g = A_{th} K Y \sqrt{2 g_c \rho_g \Delta P_g}$$

where

A_{th} venturi throat area

K flow coefficient

Y expansion factor

For steady flow conditions, the quality of the mercury leaving the boiler is equal to the ratio of the mercury vapor flow rate leaving the boiler to the liquid mercury flow rate entering the boiler. The experimentally determined quality varied from 0.96 to 1.06. Considering experimental error and this experimental data band the quality into the test section was assumed to be 100 percent for all conditions and the vapor flow rate, measured by the venturi, was used in all calculations where total mercury flow rate was required.

The heat balance across the test section varied from 0.95 to 1.09 using the NaK side as the reference.

The condenser pressure traces for condensing lengths of 15 and 34 inches are presented in figure 14. The absolute pressures were obtained by adding the differential pressure measurements to the reference manifold pressure, which was maintained constant for any run. The absolute static-pressure variation about the mean value was less than 5 percent of the mean value.

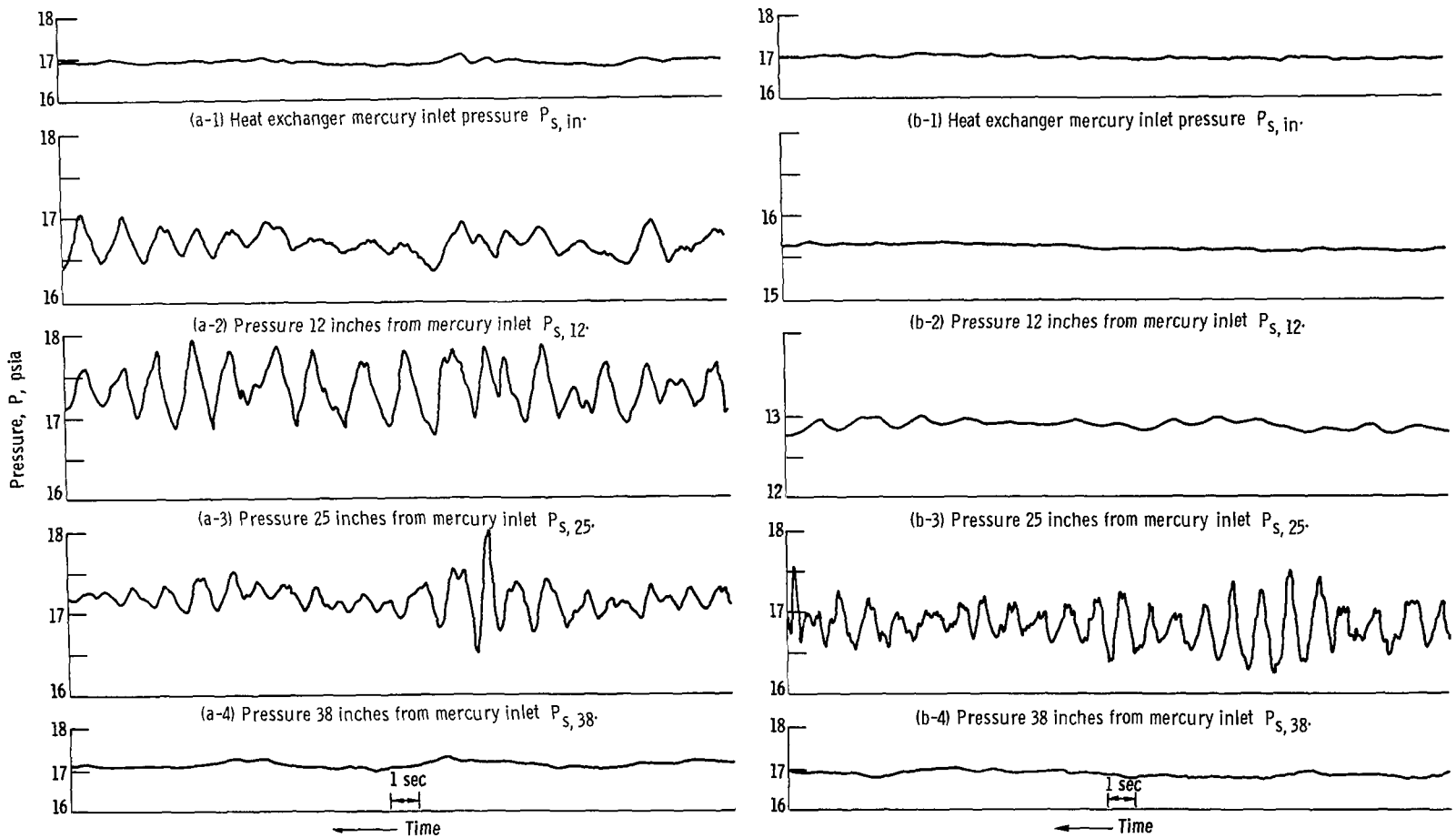

(a) Run 22; condensing length, 15 inches.

(b) Run 44; condensing length, 34 inches.

Figure 14. - Local condenser static-pressure traces.

REFERENCES

1. Lockhart, R. W.; and Martinelli, R. C.: Proposed Correlation of Data for Isothermal Two-Phase, Two-Component Flow In Pipes. Chem. Eng. Progr., vol. 45, no. 1, Jan., 1949, pp. 39-48.

2. Koestel, Alfred; Gutstein, Martin U.; and Wainwright, Robert T.: Study of Wetting and Nonwetting Mercury Condensing Pressure Drops. NASA TN D-2514, 1964.

3. Baroczy, C. J.; and Sanders, V. D.: Pressure Drop for Flowing Vapors Condensing in a Straight Horizontal Tube. Rep. No. NAA-SR-6333, Atomics International, June 1, 1961.

4. Forslund, R. P.: SNAP Mercury-Rankine Program. Mercury Condensing Experiments. Rep. No. NAA-SR-9801, Atomics International, Aug. 1, 1964.

5. Albers, James A.; and Block, Henry B.: Experimental Pressure Drop Investigation of Wetting and Nonwetting Mercury Condensing In Uniformly Tapered Tubes. NASA TN D-3253, 1966.

6. Weatherford, W. D., Jr.; Tyler, John C.; and Ku, P. M.: Properties of Inorganic Energy-Conversion and Heat-Transfer Fluids for Space Applications. (AF WADD TR-61-96), Southwest Research Institute, Nov., 1961.

7. Albers, James A.; and Namkoong, David, Jr.: An Experimental Study of the Condensing Characteristics of Mercury Vapor Flowing In Single Tubes. Paper presented at the Rankine Cycle Specialists Conference, AIAA, Cleveland, Ohio, Oct. 26-28, 1965. (Also available as NASA TM X-52151.)

8. Hays, Lance: Investigation of Condensers Applicable to Space Power Systems. Part I. Direct Condensers. Rep. No. 1588 - Final I (NASA CR-51397), Electro-Optical Systems, Inc., Aug. 15, 1962.

9. McAdams, William H.: Heat Transmission. Third Ed., McGraw-Hill Book Co., Inc., 1954.

10. Anon.: Flow Measurement. Part 5, ch. 4 of Power Test Codes Supplements - Instruments and Apparatus. ASME PTC 19. 5. 4-1959.

"The aeronautical and space activities of the United States shall be conducted so as to contribute . . . to the expansion of human knowledge of phenomena in the atmosphere and space. The Administration shall provide for the widest practicable and appropriate dissemination of information concerning its activities and the results thereof."

—NATIONAL AERONAUTICS AND SPACE ACT OF 1958

NASA SCIENTIFIC AND TECHNICAL PUBLICATIONS

TECHNICAL REPORTS: Scientific and technical information considered important, complete, and a lasting contribution to existing knowledge.

TECHNICAL NOTES: Information less broad in scope but nevertheless of importance as a contribution to existing knowledge.

TECHNICAL MEMORANDUMS: Information receiving limited distribution because of preliminary data, security classification, or other reasons.

CONTRACTOR REPORTS: Technical information generated in connection with a NASA contract or grant and released under NASA auspices.

TECHNICAL TRANSLATIONS: Information published in a foreign language considered to merit NASA distribution in English.

TECHNICAL REPRINTS: Information derived from NASA activities and initially published in the form of journal articles.

SPECIAL PUBLICATIONS: Information derived from or of value to NASA activities but not necessarily reporting the results of individual NASA-programmed scientific efforts. Publications include conference proceedings, monographs, data compilations, handbooks, sourcebooks, and special bibliographies.

Details on the availability of these publications may be obtained from:

SCIENTIFIC AND TECHNICAL INFORMATION DIVISION

NATIONAL AERONAUTICS AND SPACE ADMINISTRATION

Washington, D.C. 20546